

Visualizing the Temporal Evolution of the Universe from Cosmology Simulations

Lea Fritsch^{*}

Irene Baeza Rojo[†]

Tobias Günther[‡]

Department of Computer Science, ETH Zürich

ABSTRACT

Cosmological simulations of the universe shed light onto the formation of galactic structures. In the context of the IEEE Scientific Visualization Contest 2019, we developed a number of visualizations that concentrate on the temporal and spatial evolution of different galactic particle types, such as stars and active galactic nuclei. We visualize the interplay with scalar attributes, compute derived quantities and visualize flow properties that are governed by the attracting galactic web. The combination of multiple visualizations provides complementing views onto different aspects of the data.

Index Terms: Cosmology—Scientific visualization—Flow visualization—3D;

1 INTRODUCTION

Cosmology simulations aim to recreate the evolution of the universe to better understand its origin, its unfolding to the present day and its future development. The IEEE Scientific Visualization Contest 2019 was dedicated to the visual analysis of a recent cosmology simulation that contains 524,289 particles that unfolded over a life span of 5 million years. The simulation comprises various types of objects, including star-forming objects, stars, active galactic nuclei (AGN), wind particles and a large body of further baryons and non-baryons. The visualization is quite challenging due to the wide spectrum of scalar attributes associated with the data, including internal energy, temperature, gravitational potential and others. In our visualizations, we gradually build up the complexity, starting from particle animations in which the various particle types are color-coded. Using a chord visualization, we provide an overview of all type transitions and their frequency throughout the entire simulation period. The interplay of particles and their response in the associated scalar fields can be explored by utilizing direct volume rendering. Interpolation of the local velocity field gives an approximation to the overall motion field from which further scalar attributes, such as divergence and vorticity, are calculated. We continue with the vector field visualization by advancing from the Eulerian to a Lagrangian perspective, studying the global attractors of the system using finite-time Lyapunov exponents. The formation of galaxies is driven by gravity, which causes particles to form groups, which in turn merge over time into more massive objects. Using the above machinery and a density-based clustering, we study one cluster formation in more detail: (1) the increase in temperature during the join event, (2) the topological formation using contour trees, and (3) the temporal evolution of cluster attributes.

2 CONTEST DATA

The contest data was simulated with the Hardware/Hybrid Accelerated Cosmology Code (HACC) [7], which was extended to model

baryonic matter [6] and active galactic nuclei (AGN). The 524,289 particles are grouped into baryons and non-baryons. Baryon particles are categorized into star, star-forming, wind particle, and other. Non-baryon particles, on the other hand, are the AGN and other (e.g., dark matter). The data is given as time series of point sets with various scalar attributes. The spatial domain spans an area of $[0, 64]^3 Mpc/h$ with scale factor $h = 0.71$ and the temporal domain covers a red shift range from $z = 200$ (5 million years old) to $z = 0$ (today). The time axis is sampled linearly in the scale factor $a \in (0, 1]$, which relates to the red shift z via $a = 1/(z+1)$.

3 VISUALIZATIONS

We employed a number of information and scientific visualization methods. The following sections introduce the visualizations of the particle types, their attributes, the overall motion and the merging of particles. Afterwards, we study one galaxy formation in more detail.

3.1 Particle Types

We begin with basic visualizations of the various particle types. Throughout the paper, we color-code baryons as star (●), star-forming (●), wind particle (●), and other baryons (●). Non-baryons are color-coded as AGN (●), and other non-baryons (●).

3.1.1 Point-based Visualization

In Fig. 1, six time steps of a particle animation are shown. Seeded from a regular grid, the galactic web forms relatively quickly. Stars, forming stars, AGNs, and wind particles are rendered as large, colored spheres. To deal with occlusion, we used transparency and employed depth peeling to compose the layers in the correct order.

3.1.2 Transitions

As time progresses, the particles transition between the various types. For instance, baryonic particles may turn into star-forming particles and eventually into stars if they accumulate enough gravitational potential from nearby smaller objects. To get an overview of the frequency of transitions, we created a chord visualization, shown in Fig. 2a. In the chord visualization, a circle is divided into six sectors. Each particle type is encoded by a sector, which is connected via arcs to the other types if a transition occurred. The width of the start and end of the connecting arcs correspond to the number of outgoing transitions from either side. Note that the number of transitions is encoded per arc in logarithmic scale to cope with the vastly different value ranges. The size of the sectors is determined by the sum of those out-going connections, which is not equal to the total number of particles per type. The visualization is interactive and reveals the number of transitions as tool tip when hovering with the cursor over an arc. Some transitions are relatively common, e.g., regular baryons turning into star-forming particles. Many baryons and star-forming particles turn into wind particles and vice versa, which is indication for a strong interaction with the AGNs. Transitions between baryons and non-baryons do not occur, which is expected. Likewise, stars do not change their type once they are formed. In the chord visualization, this is visible by the zero width of their outgoing arcs.

^{*}e-mail:leaf@student.ethz.ch

[†]e-mail:irene.baeza@inf.ethz.ch

[‡]e-mail:tobias.guenther@inf.ethz.ch

To get an impression of the temporal evolution of the type distribution, we show the number of particles per type in Fig. 2b. We can see that AGNs and wind particles are tightly related. The number of stars and star-forming particles increases quickly in the beginning as many objects collide, but saturates at some point as further gravitational interactions become rarer. The number of stars increases monotonically.

3.2 Particle Attributes

Next, we concentrate on the particle attributes, e.g., internal energy U in $[\frac{km^2}{s^2}]$, density ρ in $[\frac{h^2 m_{solar}}{Mpc^3}]$ with m_{solar} being the mass of the Sun, and gravitational potential ϕ (in internal code units). Further, we have mass m (in internal code units), SPH smoothing length H in $[\frac{Mpc}{h}]$ and molecular weight μ (dimensionless), cf. Habib et al. [7].

3.2.1 SPH Interpolation

The data is given at discrete positions only. To enable direct volume rendering, we interpolated all attributes onto a 128^3 grid using the provided SPH kernel. Let a_i be the attribute at position \mathbf{x}_i and i be the particle index, then the attribute at \mathbf{x} is computed via:

$$a(\mathbf{x}) = \sum_i a_i \cdot W_H(\|\mathbf{x}_i - \mathbf{x}\|) \quad (1)$$

where $W_H(r)$ is the isotropic Wendland C^4 kernel (WC4) with smoothing length H , cf. Beck et al. [3]:

$$W_H(r) = \begin{cases} \frac{495}{32\pi H^3} \cdot (1 - \eta)^6 \cdot (1 + 6\eta + \frac{35}{3}\eta^2) & \eta < 1 \\ 0 & \eta \geq 1 \end{cases} \quad (2)$$

and $\eta = \frac{\|\mathbf{x}_i - \mathbf{x}\|}{H}$ is the relative distance. We also experimented with a binning of the provided data onto a regular grid. However, this is only possible for coarse resolutions since cells remain empty otherwise, resulting in poor quality compared to SPH interpolation.

3.2.2 Derived Quantities

In addition to the given attributes, we computed two derived quantities. Given the internal energy U , density ρ and the red shift z , the temperature T (in Kelvin) and the entropy S are:

$$T = 4.8 \cdot 10^5 \frac{U}{(1+z)^3} \quad S = \ln\left(\frac{T}{\rho^{2/3}}\right) \quad (3)$$

3.2.3 Comparison of Scalar Attributes

As an overview, we visualize the given scalar attributes in Fig. 3 with the associated color maps used throughout the paper. For this, we combine a direct volume rendering of the aforementioned SPH interpolated fields with a sphere visualization of the particles to show their actual location. We refer to the accompanying video for a temporal animation. We do not show mass in this figure, since all baryons (16.9% of total mass) and non-baryons (83.1% of total mass) had a constant mass throughout the simulation. Derived properties such as temperature and entropy are shown in Figs. 4a–4b. All attributes form the characteristic galactic web. Interestingly, the gravitational potential is positive at the outer regions of the simulation domain. Our hypothesis for the cause of this behavior is that two or more massive gravitational sources may tuck in opposite directions on a small particle. From the perspective of the small particle, we would see a local expansion, which is the opposite of the attraction usually associated with a negative gravitational potential. A confirmation of the hypothesis will require further discussion with domain scientists. Next, we concentrate on the formation of the galactic web through flow visualization.

3.3 Visualization of Motion

Each particle is equipped with a velocity vector. Using the above SPH interpolation, we compute a continuous vector field, which provides the basis for flow visualization methods that shed light on the general motion trends. For this, the velocity units are converted to be consistent with the spatial and temporal domain. With $1 Mpc = 3.086 \cdot 10^{19} km$, scale factor $h = 0.71$ and $1 A = 5 \cdot 10^6 years$, we get:

$$\left[\frac{Mpc/h}{A}\right] \approx \left[\frac{km}{s}\right] \cdot 3.628224 \cdot 10^{-6} \quad (4)$$

We use A here as the unit of the cosmological scale factor a .

3.3.1 Eulerian Properties

First, we use the vector field $\mathbf{v} = (u, v, w)$ to compute derived differential properties, such as the divergence and the curl:

$$\text{div } \mathbf{v} = \frac{\partial u}{\partial x} + \frac{\partial v}{\partial y} + \frac{\partial w}{\partial z}, \quad \text{curl } \mathbf{v} = \begin{pmatrix} \frac{\partial w}{\partial y} - \frac{\partial v}{\partial z} \\ \frac{\partial u}{\partial z} - \frac{\partial w}{\partial x} \\ \frac{\partial v}{\partial x} - \frac{\partial u}{\partial y} \end{pmatrix} \quad (5)$$

The divergence is in high correlation with the attraction exerted by the high gravitational potential. The curl magnitude is a vortex measure that shows where gravitational objects swirl around each other as they are attracted. Examples can be seen in Figs. 4c–4d.

3.3.2 Lagrangian Properties

A derived measure for the analysis of particle transport is the finite-time Lyapunov exponent, which captures the repelling and attracting behavior of hyperbolic Lagrangian coherent structures [8]. The FTLE field normalizes the spectral norm of the right Cauchy-Green tensor, which linearly estimates the maximal expansion of a virtual sphere during transport:

$$\text{FTLE}(\mathbf{x}) = \frac{1}{|\tau|} \ln \sqrt{\lambda_{\max} \left(\frac{\partial \phi_{t_0}^\tau(\mathbf{x})}{\partial \mathbf{x}} \right)^T \frac{\partial \phi_{t_0}^\tau(\mathbf{x})}{\partial \mathbf{x}}} \quad (6)$$

where $\phi_{t_0}^\tau(\mathbf{x})$ is the flow map that maps a particle seeded at point \mathbf{x} and time t_0 to its reached location after an integration of duration τ . Applied to our SPH-interpolated vector field, forward FTLE shows repelling structures (bubbles of expansion) and backward FTLE shows attracting structures (the galactic web). In Figs. 5a–5b, we computed the FTLE field over the full temporal domain on a regular grid. Fig. 5c shows the backward integration with a recent Monte Carlo rendering method [2] that models the volume rendering as a light transport problem. LCSs are typically a very effective tool to find structures that order the flow.

3.4 Temporal Evolution

In the following, we study the temporal evolution in more detail, using trajectory plots and histograms.

3.4.1 Clustering of Trajectories

Over time, the galaxies join and split. We use a density-based clustering that connects stars and AGNs within a certain distance, for which we empirically chose a threshold of $0.04 [Mpc/h]$. This is equivalent to the DBSCAN algorithm [5] with a minimum number of points set to 1, i.e., every point is a core point on its own. To look at the spatial embedding, we render the trajectories of stars and AGN particles as tubes with a fixed radius in Fig. 6a. Here, the color denotes the cluster ID. If a trajectory is selected, the radius of the tube is increased. A zoom-in is shown in Fig. 6b. We can see that when two clusters approach each other, they might oscillate, which leads to a sequence of join and split events until the clusters eventually join, escape each other, or assume an orbiting configuration.

3.4.2 Temporal Evolution of Histograms

To study the temporal evolution of scalar attributes, we plot histograms for different time steps in Fig. 7, showing stars, forming stars, AGNs and wind particles. We see that internal energy, density and temperature increase, whereas gravitational potential decreases. Fig. 8a includes baryons and non-baryons as well, showing the evolution of the gravitational potential. By making time an additional spatial dimension, we create a 2D histogram in Fig. 8b. We can see that objects with high gravitational potential increase their potential faster than smaller objects, which is likely to be caused by their larger impact on the surrounding. In general, the gravitational potential of all objects tends to increase, which slows down over time as the number of clusters increases, leaving less free objects to bind gravitationally. It is very interesting to see the final distribution of the gravitational potential at the last time step. Certain values seem to be more common, which is likely to be a stochastic effect. If the same simulation was repeated more times with slightly different initial conditions, we might end up with a different distribution. Whether there are preferential distributions or not, and how this relates to the ratio of baryons and non-baryons, could be an interesting topic to investigate in the future.

3.5 Case Study

In the following, we look at one particular region of the domain, i.e., the large red cluster in Fig. 6a.

3.5.1 Temperature Change during Join Event

In Fig. 9a, we visualize the temporal evolution of an associated scalar field during a join event. As the masses approach each other, the concentration of energy increases, which likewise causes an increase in temperature, cf. Eq. (3). This correlation provides opportunities for more sophisticated filtering operations. For instance, join events might be queried that go along with a very rapid change in temperature (high time partial). The following subsections discuss the temporal evolution of the same two clusters in more detail.

3.5.2 Topological Analysis using Contour Trees

To visualize the temporal evolution, we compute a contour tree [4], which is obtained by combing a join tree and a merge tree. For this, all split and merge events are embedded in a graph. An example of the contour tree is shown for two examples in Fig. 9b. In such cosmological simulations, contour trees can be very helpful to understand the origin of material that eventually formed a certain galaxy. For this, one would simply pick the requested node and traverse the tree backward in time, i.e., downward.

3.5.3 Dips in Per-Cluster Scalar Attribute Plots over Time

To study the temporal evolution of clusters and their associated scalar attributes, we create plots over time. In the plots, discontinuities are apparent, which correspond to two types of events: (1) join or split events of existing clusters, or (2) joining of further particles into a cluster. The former can be seen in Fig. 9d (left), where the evolution of the same attribute is shown for two different clusters. The moment, one of the cluster IDs vanishes (i.e., when it merged with the other cluster), their scalar values combine, causing a discontinuity. An example for the latter occurs when for instance an AGN particle joins an existing cluster. In Fig. 9d (right), the presence of an AGN in a cluster is shown as a dot on the line plot, which shows their correlation.

4 IMPLEMENTATION

To implement our interactive visualization tool, we chose to use open source packages. For most visualizations, we used the Visualization Tool Kit 8.2 [10] and for the user interface we used Qt 5.13 [1]. Scalar field visualizations can be generated from single time slices, making them readily available for in-situ processing. The SPH

interpolation is thereby the most expensive step. Statistical particle information, i.e., histograms, chord visualization, and time plots, need access to the full time series. Since they have low memory requirements, they can be formed along with the simulation. Further, they only need a single linear reading pass, making them suitable for in-situ processing as well. They could be viewed up to the simulation time or after the simulation is completed.

5 CONCLUSION

In this work, we visually analyzed a cosmological simulation of about half a million baryon and non-baryon particles. We displayed the temporal evolution of the particles with animations and visualized their type transitions using a chord visualization. Over time, the particles interact, which is mirrored in the associated and further derived scalar fields. To visualize the movement of particles in 3D, we employed Eulerian and Lagrangian flow visualization methods, including divergence, curl magnitude and finite-time Lyapunov exponents. The latter revealed bubbles of expansion and the attracting galactic web. Over time, the particles interact with each other due to gravitational attraction. Using a density-based clustering, we studied the increase in temperature during a join event, the topology of joins and splits using a contour tree, and the temporal evolution of scalar cluster attributes.

In the future, we would like to improve the readability of our contour trees, for which we would like to employ more advanced graph layout algorithms, such as the Reingold-Tilford [9] algorithm. To improve the clustering of large galaxies, we would like to experiment with spatially-varying minimum number of particles for the DBSCAN algorithm [5]. The SPH interpolation can cause overshooting, leading for instance to a negative entropy. At the moment, we clamped those obvious outliers away, but in the future it would be interesting to study other interpolators. To increase the frame coherence in the animations of SPH-interpolated values, it would be imaginable to interpolate not only in space, but also in time.

REFERENCES

- [1] Qt. www.qt.io. Accessed: 2019-08-12.
- [2] I. Baeza Rojo, M. Gross, and T. Günther. Accelerated Monte Carlo rendering of finite-time Lyapunov exponents. *IEEE Transactions on Visualization and Computer Graphics (Proc. IEEE Scientific Visualization 2019)*, 2020.
- [3] A. M. Beck, G. Murante, A. Arth, R.-S. Remus, A. F. Teklu, J. M. F. Donnert, S. Planelles, M. C. Beck, P. Frster, M. Imgrund, K. Dolag, and S. Borgani. An improved SPH scheme for cosmological simulations. *Monthly Notices of the Royal Astronomical Society*, 455(2):2110–2130, 11 2015. doi: 10.1093/mnras/stv2443
- [4] H. Carr, J. Snoeyink, and U. Axen. Computing contour trees in all dimensions. *Computational Geometry*, 24(2):75–94, 2003.
- [5] M. Ester, H.-P. Kriegel, J. Sander, X. Xu, et al. A density-based algorithm for discovering clusters in large spatial databases with noise. In *Kdd*, vol. 96, pp. 226–231, 1996.
- [6] N. Frontiere, C. D. Raskin, and J. M. Owen. CRKSPH – A conservative reproducing kernel smoothed particle hydrodynamics scheme. *Journal of Computational Physics*, 332:160 – 209, 2017. doi: 10.1016/j.jcp.2016.12.004
- [7] S. Habib, A. Pope, H. Finkel, N. Frontiere, K. Heitmann, D. Daniel, P. Fasel, V. Morozov, G. Zagaris, T. Peterka, V. Vishwanath, Z. Luki, S. Sehrish, and W.-K. Liao. HACC: Simulating sky surveys on state-of-the-art supercomputing architectures. *New Astronomy*, 42:49–65, 8 2016. doi: 10.1016/j.newast.2015.06.003
- [8] G. Haller. Lagrangian coherent structures. *Annual Review of Fluid Mechanics*, 47:137–162, 2015.
- [9] E. M. Reingold and J. S. Tilford. Tidier drawings of trees. *IEEE Transactions on software Engineering*, (2):223–228, 1981.
- [10] K. M. Will Schroeder and B. Lorensen. *The Visualization Toolkit*. Kitware, 4th ed., 2006.

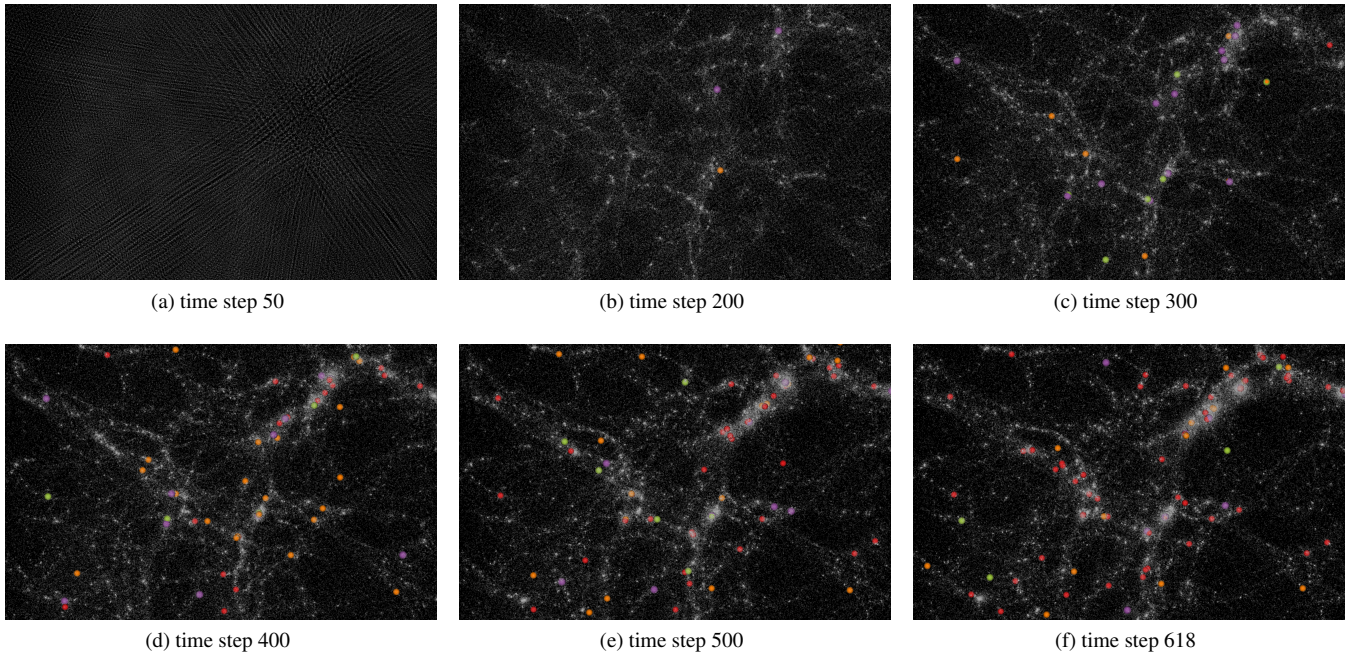


Figure 1: An overview of the various particle types at six selected time steps in the cosmology simulations. For clarity, only stars (●), forming stars (●), AGNs (●), and wind particles (●) are color-coded. Other baryons and non-baryons are shown as white dots to provide context. Over time, the characteristic galactic web is forming with a high particle concentration around AGNs and massive stars.

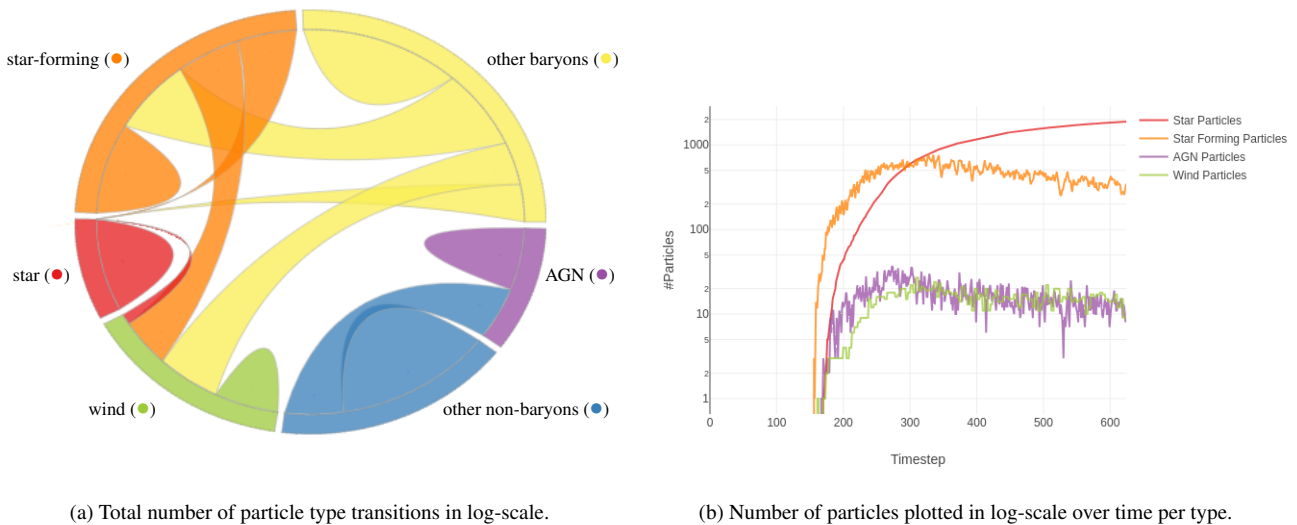
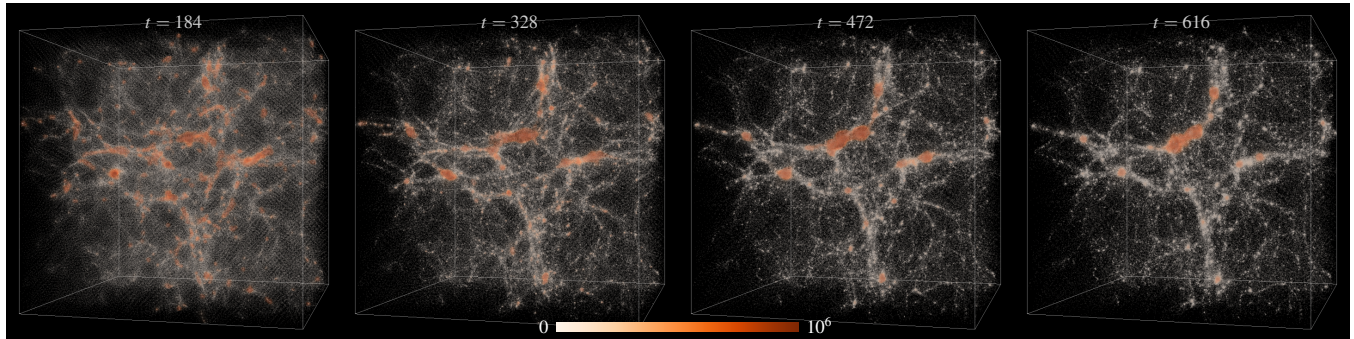
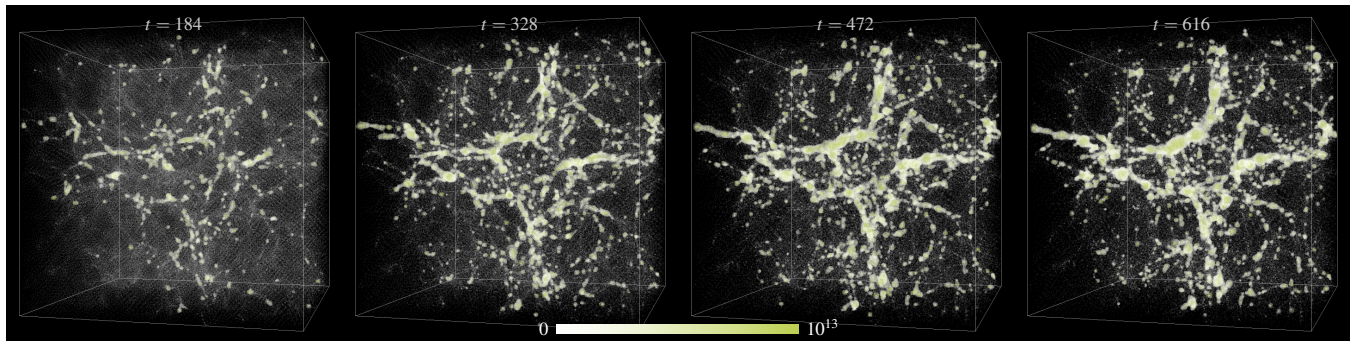


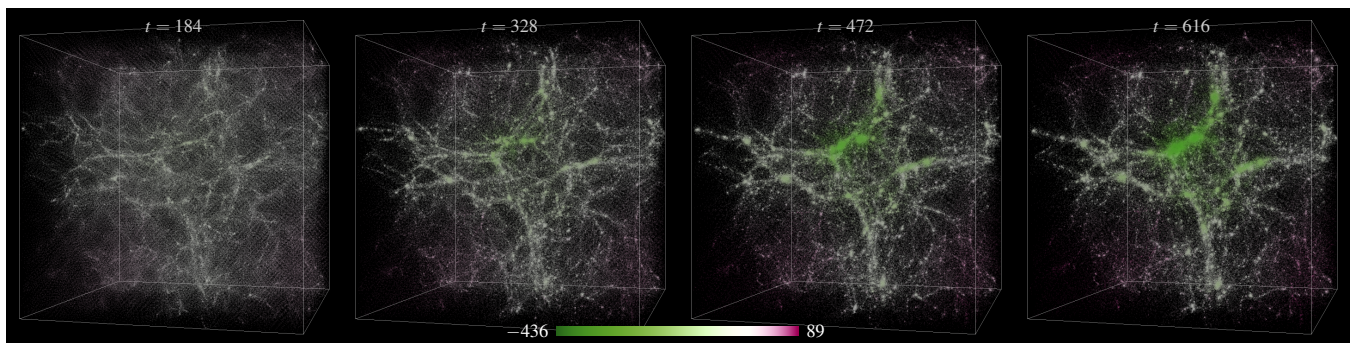
Figure 2: In (a), a chord visualization is shown, which displays the total number of type transitions throughout the entire simulation. Each arc connects two types, or it connects back to itself. The width of both arc endings encodes the respective number of outgoing transitions. Note that the chord does not display the number of incoming transitions (which is equal to the number of outgoing transitions on the other end of the arc). In (b), the total number of particles are shown for each type as a function of time, which gives an impression of the temporal evolution.



(a) Internal Energy U

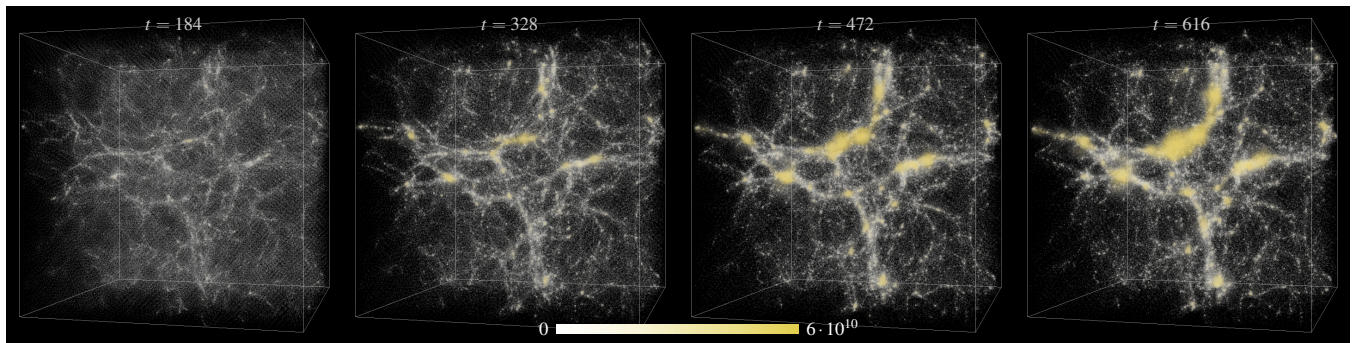


(b) Density ρ

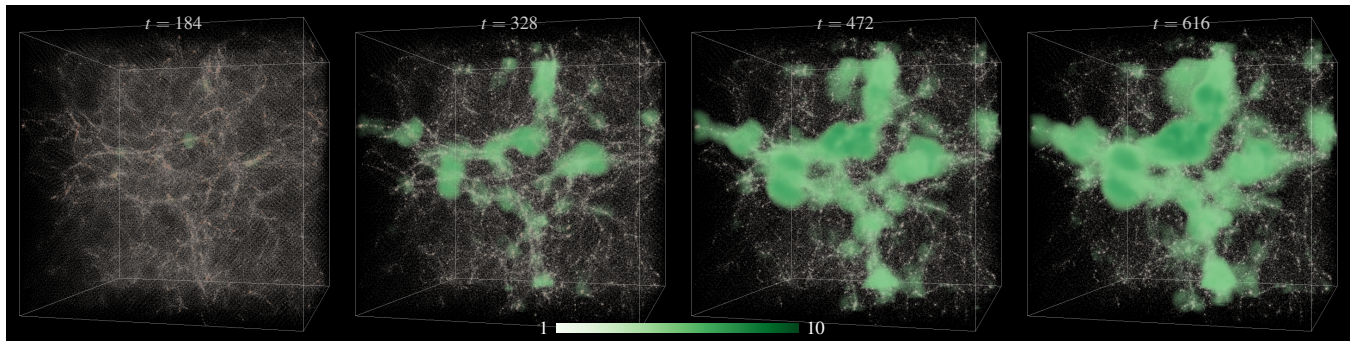


(c) Gravitational potential ϕ

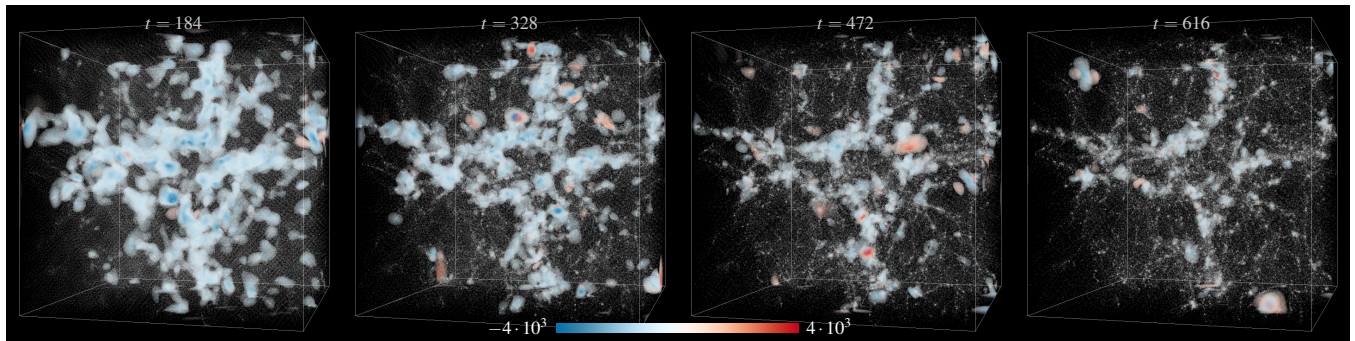
Figure 3: These visualizations show three of the given attributes in the entire domain at four selected time steps. The full sequence is found in the accompanying video. Over time, the galactic web is forming. Places of high internal energy also become locations of high density and negative gravitational potential.



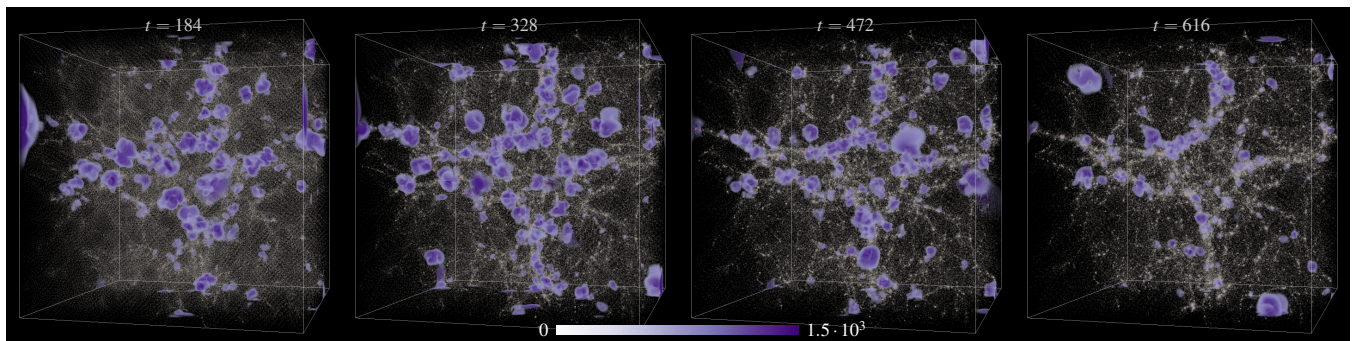
(a) Temperature T



(b) Entropy S

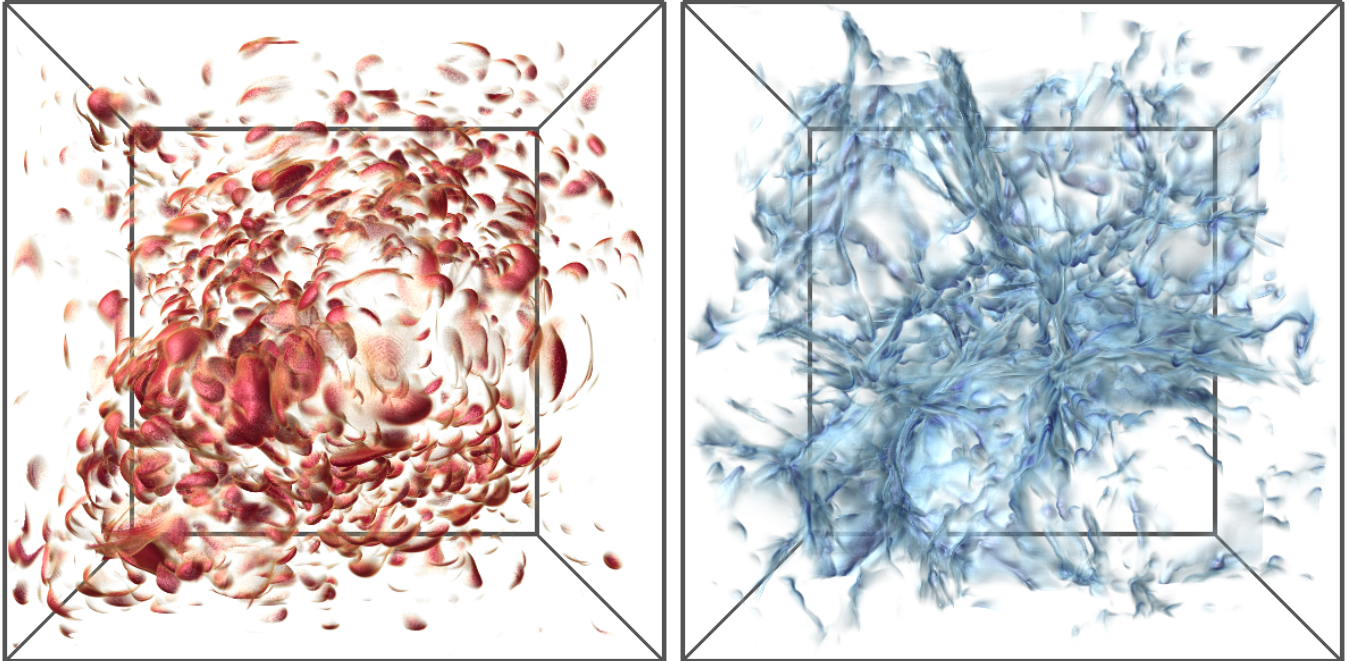


(c) Divergence $\text{div } \mathbf{v}$



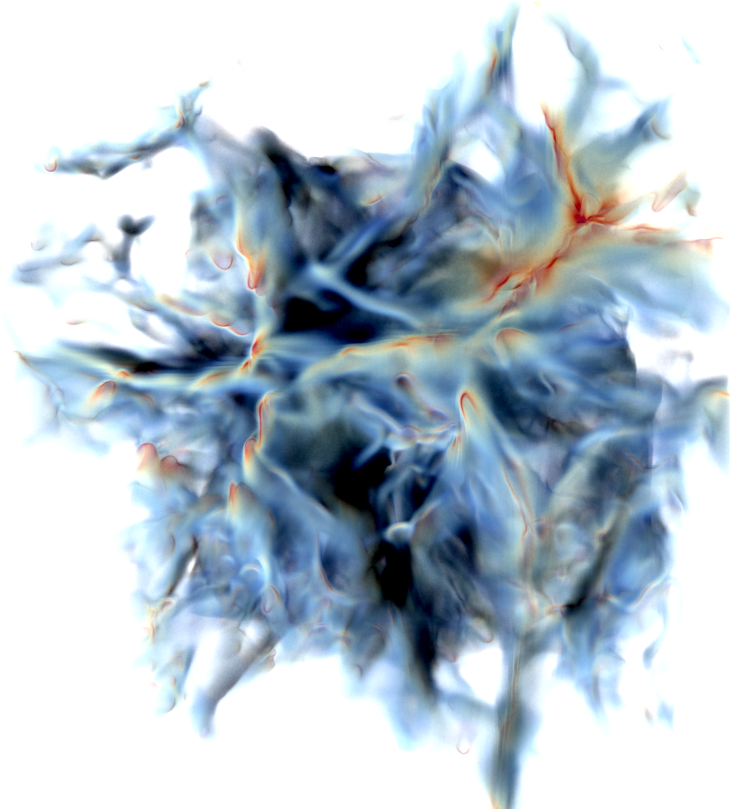
(d) Curl magnitude $|\text{curl } \mathbf{v}|$

Figure 4: This figure shows derived attributes that we computed from the given data. The first two rows show temperature and entropy, whereas the bottom two rows show Eulerian vector field properties, namely divergence and the curl magnitude, also known as vorticity. Unlike all other attributes, divergence and curl become more localized over time, as the galactic web is contracting. Note that divergence identifies expansion (positive) and contraction (negative).



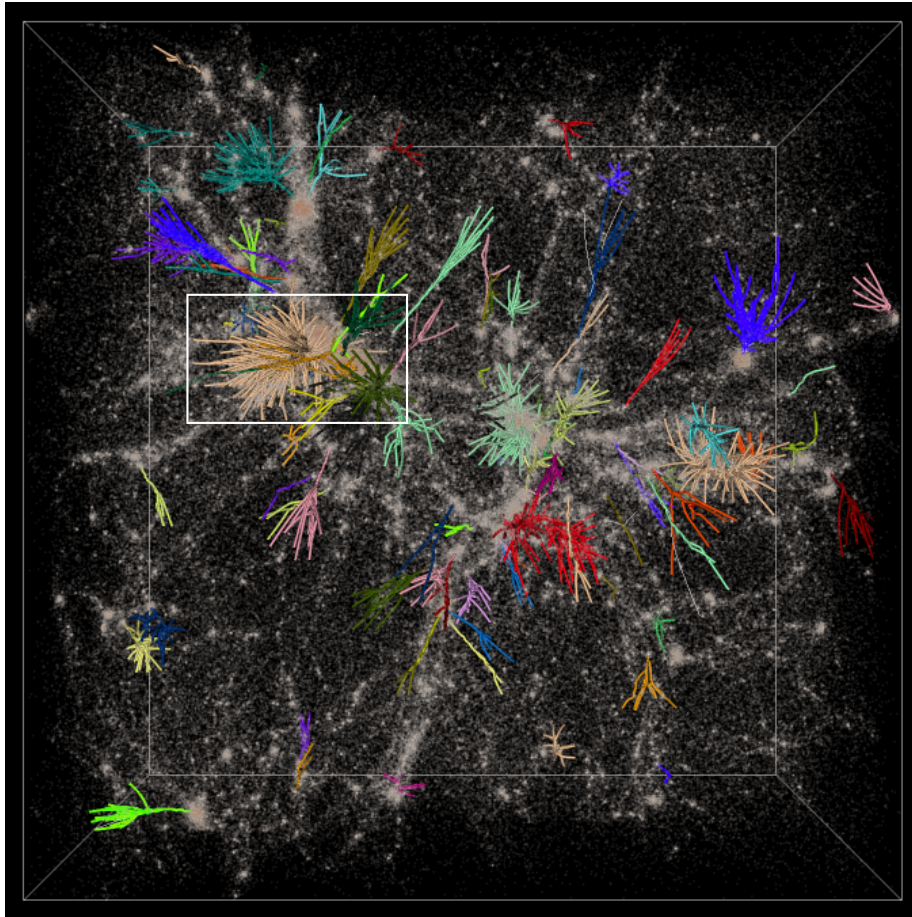
(a) Forward FTLE (repelling LCS)

(b) Backward FTLE (attracting LCS)

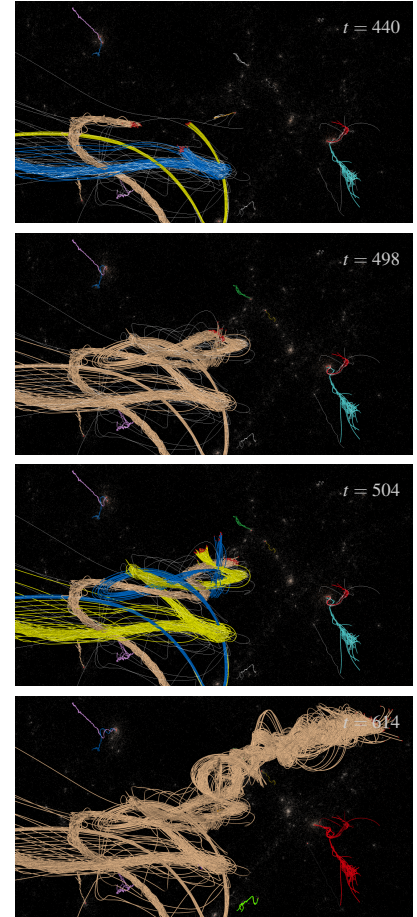


(c) Monte Carlo rendering of backward FTLE. The larger the attraction, the more red is visible.

Figure 5: Visualization of hyperbolic Lagrangian coherent structures (LCS). The forward FTLE field reveals bubbles of expansion, whereas the backward FTLE field identifies the attracting galactic web. (a) and (b) have been computed by seeding 512^3 particle trajectories from a uniform grid and tracing them over the entire time range. (c) modeled the image synthesis as a light transport problem in an inhomogeneous participating medium, which requires Monte Carlo sampling to solve. The Monte Carlo approach avoids aliasing and discretization artifacts.



(a) Overview of the entire domain at $t = 618$.



(b) Time series of three joining clusters.

Figure 6: Fig. 6a gives an overview of the particle trajectories. A zoom-in (highlighted in white) is shown in Fig. 6b, where we can see that clusters may join and split over time as they approach each other. The colors denote the cluster IDs.

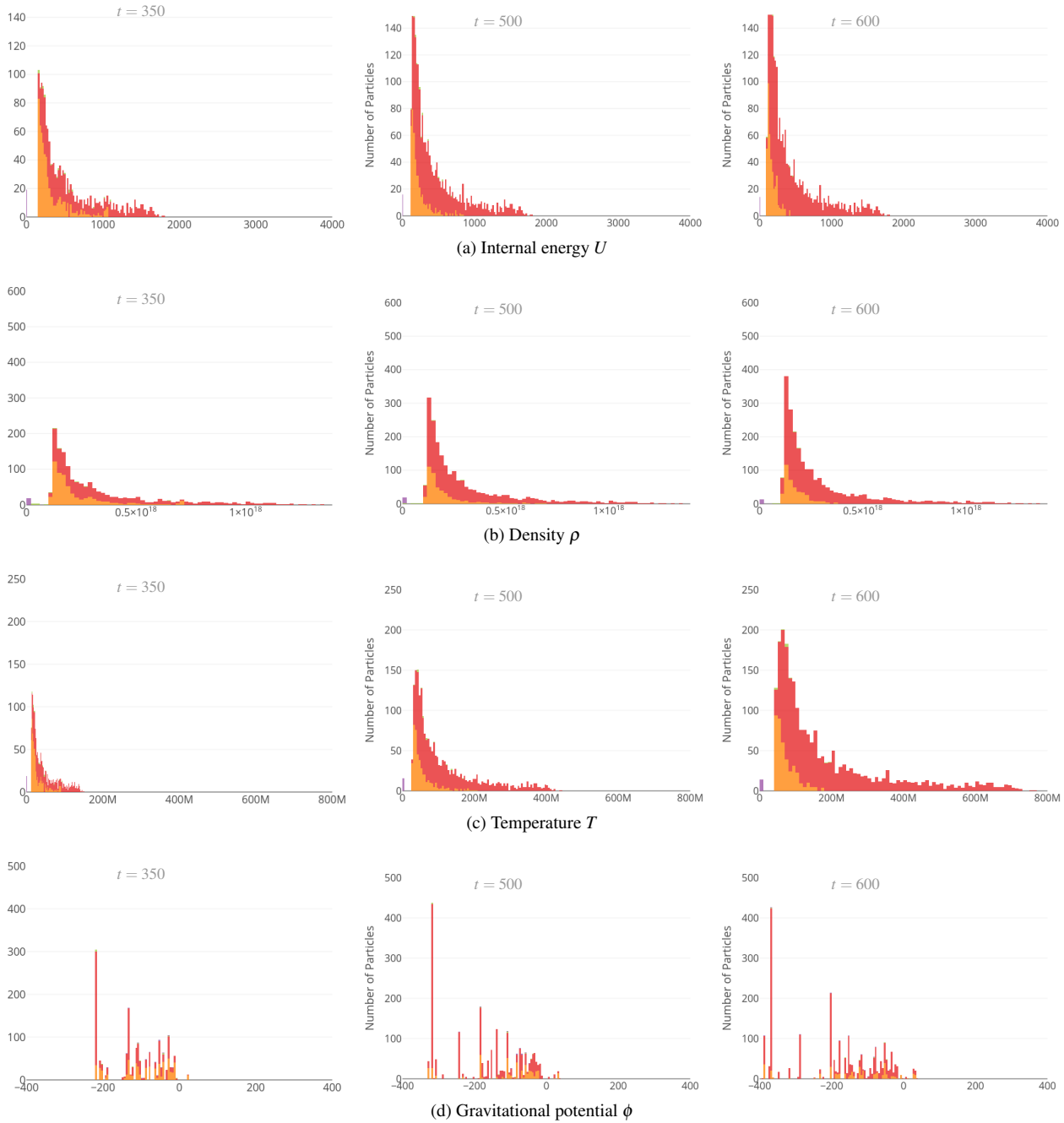


Figure 7: The scalar attributes that are associated with the particles evolve over time, as the galactic web is forming. In the above figures, only stars (●), forming stars (●), AGNs (●), and wind particles (●) are color-coded. For most attributes, the distribution of values shifts towards higher values over time; especially for the temperature. The only exception is the gravitational potential, which becomes more negative. This is expected, since objects move closer together, exerting a stronger attraction.

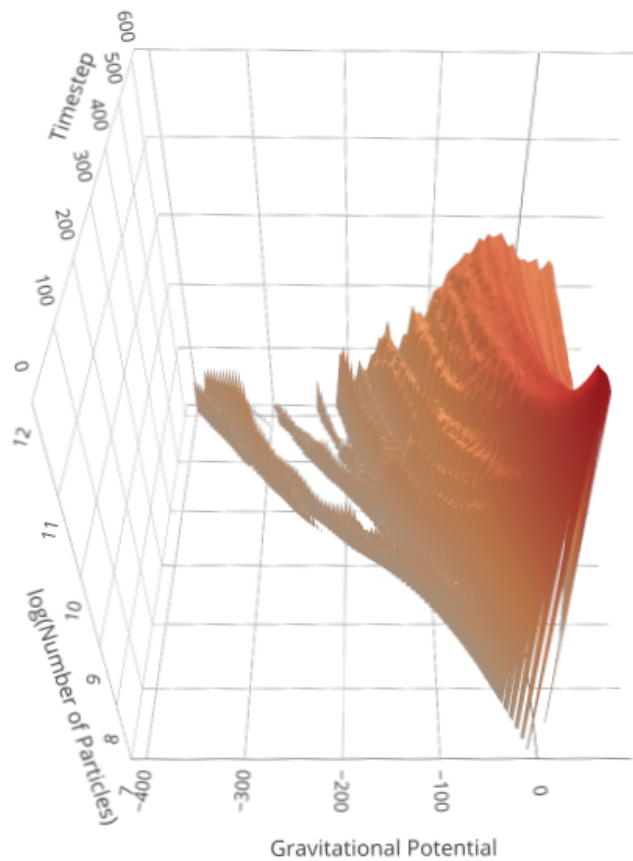
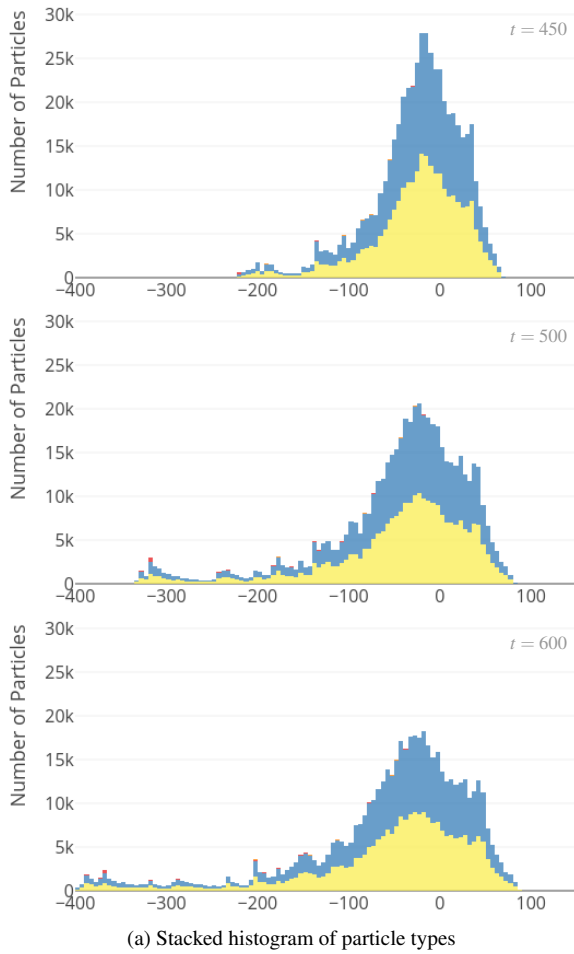
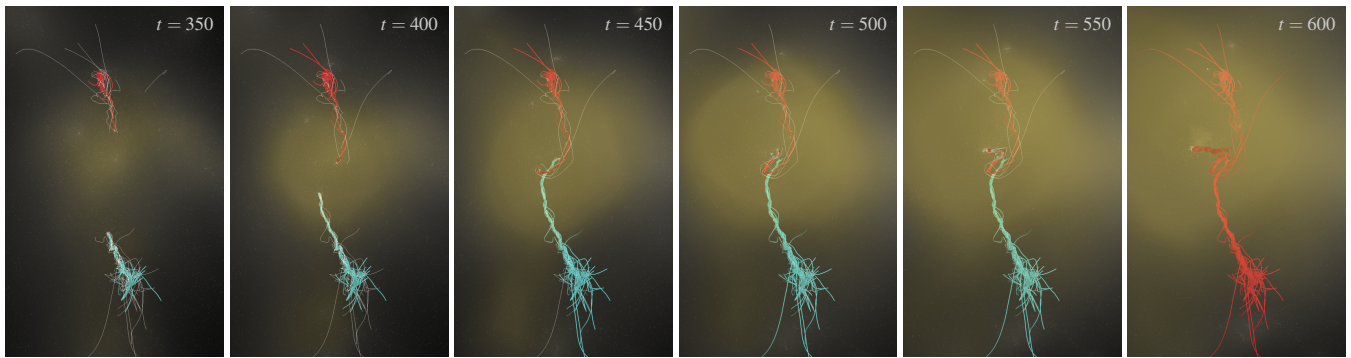
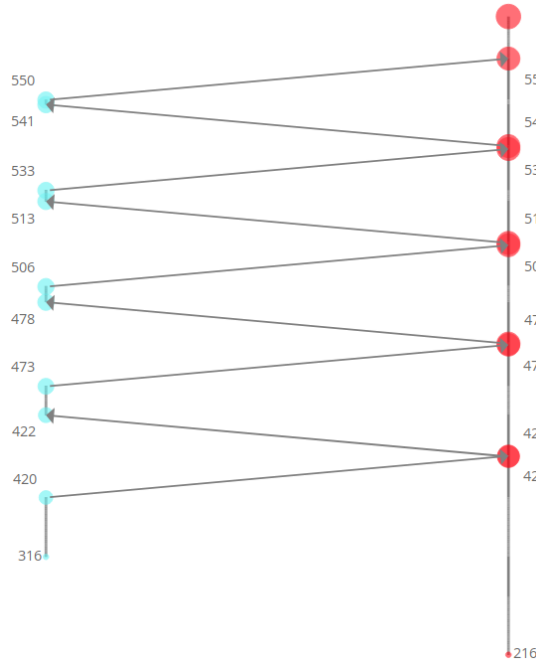


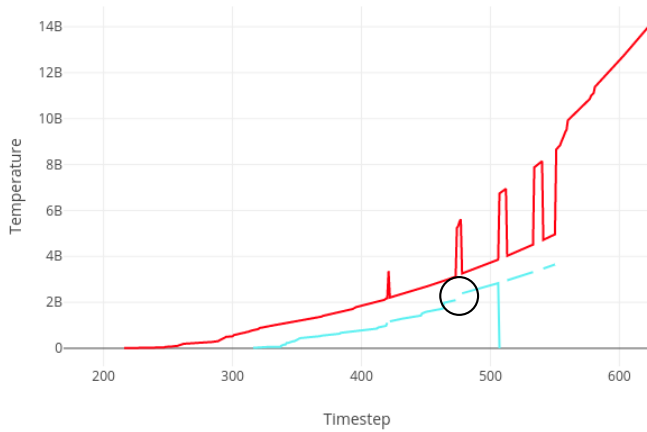
Figure 8: In 8a, stacked histograms of the gravitational potential are shown over time for all particles. As above, we color-code stars (●), forming stars (●), wind (●), and AGNs (●). Other baryons (●) and non-baryons (●) are shown as well, which are the most common particle types. The 2D histogram in 8b shows that the gravitational potential distribution drifts towards smaller values, i.e., to the left. The shift is faster, the more negative the values, which is likely to be caused by a larger gravitational impact on the surrounding. Over time, the shift towards smaller values slows down as most particles have already formed clusters, leaving less free particles to join into clusters.



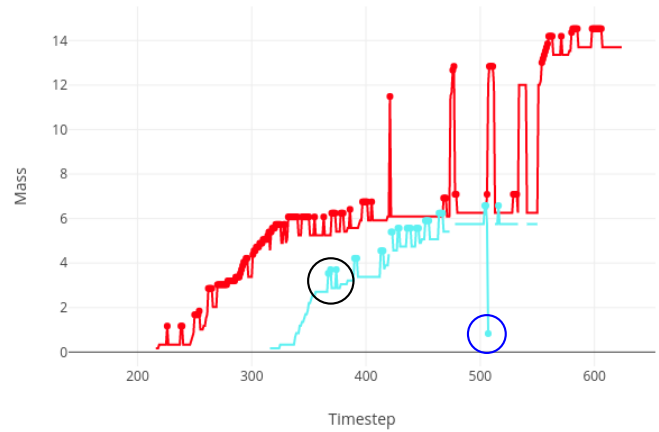
(a) Visualization of temperature during a merge event of two clusters. The temperature increases as the two clusters approach each other.



(b) Visualization of a contour tree that shows the join and merge events of the two clusters over time. The lowest dots on each line show the formation of this cluster. As time progresses, the cyan cluster repeatedly joins and splits from the red cluster. The numbers in the labels represent the time step in which the event occurred.



(c) Visualization of the temperature attribute of the two clusters in 9a. Discontinuities in one line indicate a merge event of the clusters (see the black highlighted circle). As the cyan cluster briefly merges with the red cluster, the temperature of the red cluster increases for a moment.



(d) Visualization of the mass attribute of the two clusters in 9a. In this image, the presence of an AGN is highlighted with a dot. When an AGN joins an existing cluster (black highlighted circle), the mass increases. When only a fraction of particles of the cyan cluster joins the red cluster (blue highlighted circle), the mass (and temperature) drop.

Figure 9: Case study of a particular merging event of two clusters.